

Improved model of a ball bearing for the simulation of vibration signals due to faults during run-up

Matej Tadina¹, Miha Boltežar¹

¹Faculty of Mechanical Engineering, University of Ljubljana, Aškerčeva 6, 1000 Ljubljana, SI-Slovenia

Cite as:

M. Tadina and M. Boltežar

Improved model of a ball bearing for the simulation of vibration signals due to faults during run-up. *Journal of Sound and Vibration* (2011), Volume: 300, Issue 17, Pages 4287-4301

Abstract

In this paper an improved bearing model is developed in order to investigate the vibrations of a ball bearing during run-up. The numerical bearing model was developed with the assumptions that the inner race has only 2DOF and that the outer race is deformable in the radial direction, and is modelled with finite elements. The centrifugal load effect and the radial clearance are taken into account. The contact force for the balls is described by a nonlinear Hertzian contact deformation. Various surface defects due to local deformations are introduced into the developed model. The detailed geometry of the local defects is modelled as an impressed ellipsoid on the races and as a flattened sphere for the rolling balls. With the developed bearing model the transmission path of the bearing housing can be taken into account, since the outer ring can be coupled with the FE model of the housing. The obtained equations of motion were solved numerically with a modified Newmark time-integration method for the increasing rotational frequency of the shaft. The simulated vibrational response of the bearing with different local faults was used to test the suitability of the envelope-analysis technique and the continuous wavelet transformation was used for the bearing fault identification and classification.

1 Introduction

Ball bearings are among the most important and frequently used components the electric motors; however bearings may contain manufacturing errors or mounting defects. Damage may also occur during working conditions. Such errors cause vibration, noise, and even failure of the whole system, which leads to expensive claims for damage. To avoid this and to ensure rapid and cheap production there is a need for a quick end-test of the electric motors to determine any bearing faults.

The first step in bearing-fault detection during run-up would be a numerical model for the bearing-vibration response due to faults during the run-up. A well-defined vibration signal during the run-up of a faulty bearing could be used to find a suitable method for the fault diagnostic. A lot of research work has been done to model the vibration response of a bearing due to faults at a constant rotational speed. The early work on the mathematical modelling of localised single and multiple point defects in bearings was published by McFadden and Smith [1,2]. They proposed a vibration model for point defects on the inner race of a rolling-element bearing under a radial load. In this model the vibrations due to defects are modelled as the product of a series of impulses at the rolling-element passing frequency and the amplitude of the transfer function, convolved with the impulse response of the exponential decay

function. A similar analytical model has been proposed by Tandon and Choudhury [3] for predicting the vibration frequencies of rolling bearings and the amplitudes of the significant frequency components due to localised defects on the outer race, the inner race or on one rolling element under an axial load. They extended the model further in [4], where a rotor-bearing system was modelled as a 3 DOF system, and the excitation force is modelled as periodic pulses [3]. The first mathematical model for modelling bearing vibrations was proposed by Sunnersjo [5]. The bearing was modelled as a 2 DOF system, which provides the load-deflection according to Hertzian contact theory, while ignoring the mass and the inertia of the rolling elements. The two orthogonal DOF are related to the inner race. Rafsanjani et al. [6] combined this 2 DOF model with an analytical approach to model the nonlinear dynamic behavior of a bearing due to localised surface defects. In this model the effect of the radial internal clearance was taken into account. Liew [7] presented four different bearing models in order to model bearing vibrations. The most comprehensive model includes the rolling-element centrifugal load, the angular contact and the radial clearance, and is a 5 DOF model. The 5 DOF bearing model includes not only the radial displacement of the inner race, but also the axial displacement and the rotation around the x and y axes, Figure 1. Building on the 2 DOF model developed by Liew, Feng [8] developed a bearing-pedestal model with 4 DOF, as it includes a pedestal 2 DOF. The model takes into consideration the slippage in the rolling elements, the effect of mass unbalance in the rotor and the possibility of introducing a localised fault in the inner or outer race. Arslan and Aktürk [9] developed a shaft-bearing system with bearing defects. The model has 3 DOF, 2 DOF for the radial displacement and 1 DOF for the axial displacement. The balls in the bearing have additional DOFs since they can vibrate in a radial direction. The effect of the centrifugal load on the balls is neglected. A new, comprehensive model was proposed by Sapanen and Mikkola [10, 11], which includes the effect of different geometrical faults, such as surface roughness, waviness and localised and distributed defects. The dynamic model is a 6 DOF model, which includes both the non-linear Hertzian contact deformation and the elasto-hydrodynamic fluid film. The model of the ball bearing was implemented and analysed using a commercial, multi-body software application (MSC.ADAMS).

Kiral and Kar ulle [12] modelled the outer ring and the housing with finite elements and used a radially distributed load, as given in [1]. The rotating circumferential load is applied on the nodes whenever a ball carrying a load moves over that node. A local defect is modelled by amplifying the magnitudes of the radial forces defined for the nodes that are in the defected area.

A common feature of all these models is that the rotational speed of the shaft is constant, the outer ring is rigid and is assumed to be firmly fitted to a rigid housing.

Although many researches have investigated the vibration characteristics of ball bearings due to local defects, no studies have been published on bearing vibration due to local defects during the run-up of the shaft. Hence, this paper will present an improved ball-bearing model with local faults, to simulate the vibration signal of a defective bearing during the run-up of the shaft, where the centrifugal load is taken into account and the outer ring is deformable in the radial direction. Such a simulated vibration signal of a faulty bearing will be used to test the suitability of the envelope-analysis technique and wavelet analysis for bearing-fault identification during run-up.

2 Bearing modelling

Based on previous studies [7, 13–15], a multiple-degree-of-freedom model of a radial ball bearing was developed, shown in Figure 1, to determine the vibration of a faulty bearing during run-up. The following assumptions were made:

1. The rolling elements, the inner and outer races and the rotor have motions in the plane of the bearing only.
2. The balls are assumed to have masses, and the vibrations of the balls are considered in the radial direction. The centrifugal load on the balls is taken onto account.
3. Deformations in the contact occur according to the Hertzian theory of elasticity. The effect of the elasto-hydrodynamic lubricated (EHL) contact is neglected. The inner ring is rigid. The outer ring is deformable in the radial direction and is modelled with finite elements. The finite elements are two-noded, locking-free-shear, curved beam elements, as derived in [16]

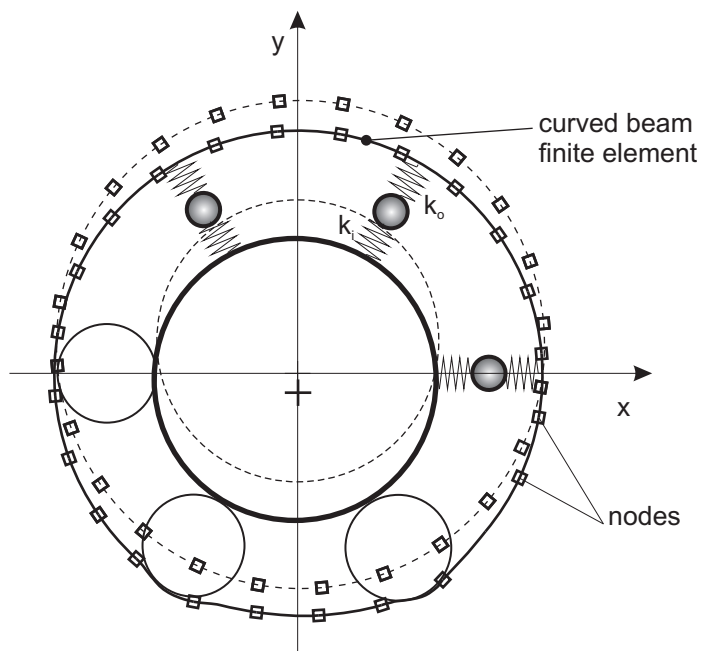


Figure 1: Developed bearing model.

4. The cage is rigid and ensures a constant angular separation between the rolling elements, and hence there is no interaction between rolling elements. The angular velocity of the cage can change over time and the velocity of the ball is changing at the same rate.
5. In the bearing model it is assumed that slipping or sliding between the components of the bearing can occur and this is given by a prescribed function in the bearing model.
6. The rollers in a rolling-element bearing are assumed to have no angular rotation about their axes, i.e. no skewing. Hence, there is no interaction of the corners of the rollers with the cage and the flanges of the races.
7. The bearings are assumed to operate under isothermal conditions. Hence, all thermal effects that might arise due to the rise in temperature, such as a change in the lubricant viscosity, the expansion of the rolling elements and the races, and the reduced endurance of the material, are considered to be absent.
8. The damping of a ball bearing is very small. This damping is present because of friction and a small amount of lubrication. An estimation of the damping of a ball bearing is very difficult because of the dominant extraneous damping, which swamps the damping of the bearing. The damping effect of the EHL contact is neglected. The damping in the proposed model is assumed to be structural damping.
9. The outer ring of the bearing is supported by a flexible housing. The housing can have asymmetric stiffness properties. This effect can be described by springs with different stiffness that are connecting nodes of curved beam elements to the supporting structure or with a finite-element model of the housing.

2.1 Equation of motion

In the mathematical modelling, the ball bearing is considered as a spring-mass system, where the rolling elements act as nonlinear contact springs and the outer race is a deformable body, as shown in Figure 2. Lagrange equations are applied to derive the equations of motion of the bearing model. Using the Lagrange equations it is necessary to calculate the total potential and kinetic energy of the system. In order to calculate the potential energy of the contact deformation, first the contact deformation of the

j -th ball at the inner and outer races has to be calculated. Since the outer race is not fixed and is deformable in the radial direction, the inner and outer contact deformations are expressed as [14]:

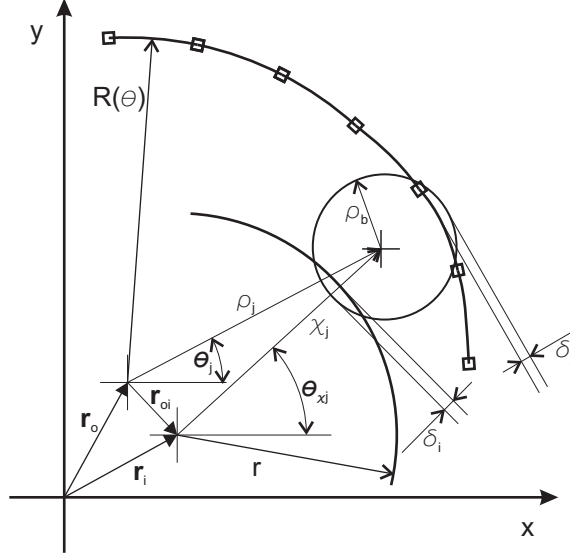


Figure 2: Positions of race and balls centres and deflection of the j -th ball-race contact.

$$\delta_{i,j} = r + \rho_b - \chi_j, \quad (1)$$

$$\delta_{o,j} = (\rho_j + \rho_b) - R(\theta_j), \quad (2)$$

The variable θ_j defines the angular position of the j th ball centre with respect to the centre of the outer race x_o and y_o , r is the radius of the inner race, ρ_j is the radial position of the j -th ball, ρ_b is the radius of the ball, x_i and y_i are the positions of the inner race, and the position of the centre of the ball from the inner race χ_j is obtained from:

$$x_i + \chi_j \cos \theta_{\chi_j} = x_o + \rho_j \cos \theta_j, \quad (3)$$

$$y_i + \chi_j \sin \theta_{\chi_j} = y_o + \rho_j \sin \theta_j, \quad (4)$$

thus:

$$\chi_j = \left((x_o - x_i)^2 + \rho_j^2 + 2\rho_j(x_o - x_i) \cos(\theta_j) + 2\rho_j(y_o - y_i) \sin(\theta_j) + (y_o - y_i)^2 \right)^{1/2}. \quad (5)$$

Since the outer ring in the proposed model is deformable, the local radius of the outer race is :

$$R(\theta_j) = R_0 + \mathbf{N}_j^e \cdot \mathbf{d}^e, \quad (6)$$

where R_0 is the radius of the non-deformed outer race, \mathbf{N}_j^e is the vector of the interpolation functions evaluated at the position in the element where the contact occurs and \mathbf{d}^e is the vector of the nodal displacements for the element.

The contact force between the inner race and the ball or the outer race and the ball arise only when there is a compression in the contact, which means that δ_i and δ_o have to be greater than 0:

$$\delta_{i,j+} = \begin{cases} r + \rho_b - \chi_j, & \text{if } r + \rho_b - \chi_j > 0 \\ 0, & \text{otherwise} \end{cases} \quad (7)$$

$$\delta_{o,j+} = \begin{cases} (\rho_j + \rho_b) - R(\theta_j), & \text{if } (\rho_j + \rho_b) - R(\theta_j) > 0 \\ 0, & \text{otherwise} \end{cases} \quad (8)$$

With a known contact deformation and following the procedure described in [17] the total potential energy is calculated as:

$$V = m_s g (y_i + y_{oi}) + \mathbf{M} \mathbf{g} \mathbf{d}_y + m_b g N_b y_o + \sum_{j=1}^{N_b} m_b g \rho_j \sin \theta_j + \frac{2}{5} \sum_{j=1}^{N_b} k_i \delta_{i,j+}^{\frac{5}{2}} + \frac{2}{5} \sum_{j=1}^{N_b} k_o \delta_{o,j+}^{\frac{5}{2}} + \frac{1}{2} \mathbf{d}^T \mathbf{K} \mathbf{d}, \quad (9)$$

where m_s is the mass of the shaft and the inner ring, \mathbf{M} is the mass matrix of the outer ring, \mathbf{d}_y is the vector of the nodal displacement with non-zero entries only on the y displacements, \mathbf{K} is the stiffness matrix of the outer ring and the supporting structure, $\delta_{i,j+}$ and $\delta_{o,j+}$ are the inner and outer deformation of balls, and $k_{i/o}$ is the stiffness coefficient at the inner and outer contacts and it depends on the geometry and the material properties of the contacting surfaces [18].

The bearing's inner ring has 2 DOFs, and taking into account the deformability of the outer ring, the total kinetic energy is thus calculated as:

$$T = \frac{1}{2} m_s (\dot{x}_i^2 + \dot{y}_i^2) + \frac{1}{2} \sum_{j=1}^{N_b} m_b (\dot{\rho}_j^2 + \rho_j^2 \dot{\theta}_j^2 + \dot{x}_o^2 + \dot{y}_o^2 + 2\dot{x}_o (-\sin \theta_j \rho_j \dot{\theta}_j + \cos \theta_j \dot{\rho}_j) + 2\dot{y}_o (\cos \theta_j \rho_j \dot{\theta}_j + \sin \theta_j \dot{\rho}_j)) + \frac{1}{2} N_b I_b \dot{\theta}_j^2 \left(1 + \frac{R_0}{\rho_b}\right)^2 + \frac{1}{2} I_s \omega_s^2 + \frac{1}{2} \dot{\mathbf{d}}^T \mathbf{M} \dot{\mathbf{d}}, \quad (10)$$

where \dot{x}_i , \dot{y}_i are the velocities of the inner race/shaft, $\dot{\rho}_j$ is the radial velocity of the j -th roller element, $\dot{\theta}_j$ is the angular position of the j -th rolling element, m_b is the mass of the rolling element, I_b is the moment of inertia of the roller element, I_s is the moment of inertia of the shaft and the inner race, ω_s is the angular velocity of the shaft, \dot{x}_o , \dot{y}_o are the velocities of the centre of the inner race and $\dot{\mathbf{d}}$ are the nodal velocities of the outer race. It should be noted that x_o and y_o are not generalized coordinates and depend on the nodal displacements \mathbf{d} and are calculated as:

$$x_o = \frac{\sum_{i=1}^{N_N} d_{xi}}{N_N}, \quad (11)$$

$$y_o = \frac{\sum_{i=1}^{N_N} d_{yi}}{N_N}, \quad (12)$$

where N_N is the number of nodes of the outer ring and d_{xi} , d_{yi} are the nodal displacements in the x and y directions at node i .

With a known total potential and kinetic energy and by applying the Lagrange equation, the equations of motion of the inner ring and the rolling elements are derived as:

$$m_s \ddot{x}_s + k_i \sum_{j=1}^N \delta_{i,j+}^{\frac{3}{2}} \frac{\rho_j \cos \theta_j + x_o - x_i}{\chi_j} = F_u \cos \theta_s \quad (13)$$

$$m_s \ddot{y}_s + k_i \sum_{j=1}^N \delta_{i,j+}^{\frac{3}{2}} \frac{\rho_j \sin \theta_j + y_o - y_i}{\chi_j} = m_s g + F_u \sin \theta_s \quad (14)$$

$$m_b \ddot{\rho}_j - \rho_j \omega^2 + k_o \delta_{o,j+}^{\frac{3}{2}} - k_i \delta_{i,j}^{\frac{3}{2}} \frac{\rho + (x_o - x_i) \cos \theta_j + (y_o - y_i) \sin \theta_j}{\chi_j} = -m_b g \sin \theta_j - m_b (\ddot{x}_o \cos \theta_j + \ddot{y}_o \sin \theta_j) \quad (15)$$

And for the outer ring, since the finite elements are used:

$$\mathbf{M} \ddot{\mathbf{d}} + \mathbf{C} \dot{\mathbf{d}} + \mathbf{K} \mathbf{d} = \mathbf{F}_m \quad (16)$$

where \mathbf{M} is the structural mass matrix, \mathbf{K} is the structural stiffness matrix and \mathbf{F}_m are the nodal forces in the finite-element model and \mathbf{d} is the displacement vector, and dot notation is used to denote the differentiation with respect to time. \mathbf{C} is the structural damping matrix, which is additionally introduced as the equivalent Rayleigh damping:

$$\mathbf{C} = \alpha \mathbf{M} + \beta \mathbf{K} \quad (17)$$

Because the location of the contact forces between the outer ring and the rolling element moves on the beam element, the moving load formulation within the element has to be used. The moving load vector \mathbf{F}_m for the outer ring is formulated as:

$$\mathbf{F}_m = \sum_{j=1}^N \mathbf{N}_j^T F_{o,j}, \quad (18)$$

where \mathbf{N}_j^T is the transposed vector of the interpolation functions, $F_{o,j}$ is the contact force on the outer race at the j -th ball. Using the equations (2) and (6) the outer contact force at the j -th ball can be written as:

$$F_{o,j} = k_o (\rho_j + \rho_b - (R_0 + \mathbf{N}_j \mathbf{d}))^{\frac{3}{2}}, \quad (19)$$

where \mathbf{N}_j is the vector of the shape functions evaluated at the position of the ball's outer-race contact. It should be noted that \mathbf{N}_j is a vector with zero entries, except those corresponding to the curved beam nodal displacement on which the contact of the j -th ball occurs. Thus for a curved beam element with six degrees of freedom, the number of non-zero entries within a $1 \times n$ vector will be six, where n is the total degrees of freedom in the finite+element model of the outer race. The values of this 1×6 subvector are dependent on the application point of the contact within an element. Since the loads in the finite-element model can be applied only at nodes, the point contact force must be reduced to the equivalent nodal forces and moments. When the contact point moves to another position, the numerical values of the interpolation functions change, and consequently, the equivalent nodal loads vary accordingly. It should be apparent that when the contact point moves to an adjacent element the interpolation functions of the new element must be used.

The equations (13)-(16) are nonlinear, coupled, ordinary differential equations and a modified, explicit Newmark method can be used to solve them.

3 Modelling of faults

At an early stage of the bearing's operation almost only local defects are present due to the improper mounting of the bearing, which will cause a dent due to the plastic deformation of the rolling surface. Another local defect may be present in the bearing due to debris, since grease in the bearing can contain particle contaminants. Such particle contaminant can be modelled as a local defect with the exception that the particle is free to move within the bearing. Most of the presented models of bearing faults [6, 8, 9] assume that the rolling element will lose contact suddenly once it enters the dent region, and will regain contact instantly when exiting that area. In this way the modelling results in very large impulsive forces in the system and as a consequence the acceleration increases sharply in order to maintain the balance within system. In order to model the behaviour of the rolling element so as to reflect the actual path that the rolling element takes while rolling into and out of the dent, the dent was modelled as an ellipsoidal depression on the inner and outer races, while the dent on the rolling element was modelled as a flattened sphere. Another important aspect of this model is that due to the different geometry of the contact between the dent and the bearing component the contact-stiffness changes due to the different geometrical properties in the contact.

3.1 Outer-race defect

Let there be a defect on the surface of the outer race at an angle φ from the horizontal axis, as shown in Figure 3. The dent has an angle length of φ_d . If the rolling-element position θ_j coincides with the dent-angle range $\varphi < \theta_j < \varphi + \varphi_D$ the contact deformation will be smaller for the dent depth D_d at the position φ_c where is the contact point C . The contact deformation between the rolling element and the dent is now calculated as:

$$\delta_{Do+} = \begin{cases} \|\rho_j + \rho_{bC}\| - (R(\varphi_C) + D_{do}(\varphi_C)) & \text{if } \|\rho_j + \rho_{bC}\| - (R(\varphi_C) + D_d(\varphi_C)) > 0 \\ 0, & \text{otherwise} \end{cases} \quad (20)$$

where D_d is the depth of the dent at the contact position φ_c . It should be noted that the contact deformation in the dent is given by simple equation (20), although behind these equations are hidden

extensive trigonometric equations, that are beyond the scope of this paper. Another important aspect of the detailed dent modelling is changing the stiffness in the contact. According to Hertzian contact theory the contact stiffness depends on the curvature sum and the difference. When the rolling element strikes a dent, the curvature properties are different to those on the race. The curvature sum and the difference for the two contacting bodies, shown in Figure 4, are expressed as [18]:

$$\sum \rho = \frac{1}{r_{I1}} + \frac{1}{r_{I2}} + \frac{1}{r_{II1}} + \frac{1}{r_{II2}}, \quad (21)$$

and

$$F(\rho) = \frac{(\rho_{I1} - \rho_{I2}) + (\rho_{II1} + \rho_{II2})}{\sum \rho}, \quad (22)$$

where ρ is the curvature and is defined as $\rho = 1/r$. For the ball's outer-race contact the radii of curvature r_i are:

$$r_{I1} = \rho_b \quad r_{I2} = \rho_b \quad r_{II1} = R_D \quad r_{II2} = R(\theta) \quad (23)$$

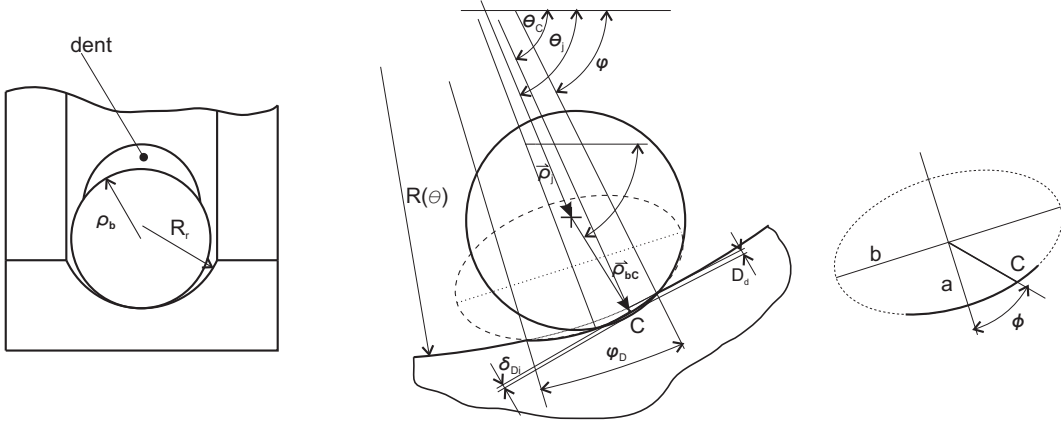


Figure 3: Contact geometry and deformation on the outer ring in a dent.

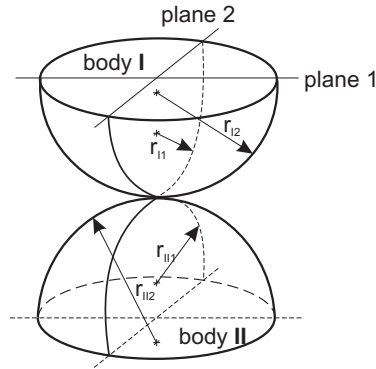


Figure 4: Geometry of the contacting bodies.

When the ball strikes into the dent, the radius of curvature r_{II2} changes:

$$r_{II2} = R_D = \frac{ab}{(a^2 \sin^2 t + b^2 \cos^2 t)^{\frac{3}{2}}}, \quad (24)$$

where a is the semi major axis, b is the semi minor axis of the ellipsoid and t is a parameter given by the polar angle ϕ from the ellipse centre as:

$$t = \tan^{-1} \left(\frac{a}{b} \tan \phi \right) \quad (25)$$

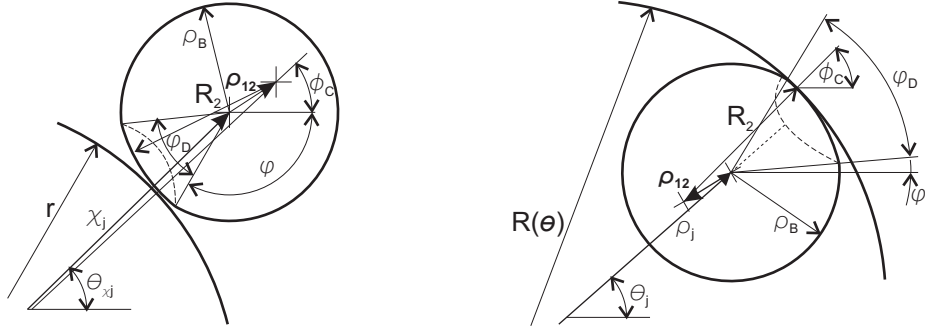


Figure 6: Dent on the rolling element. (a) Contact between the inner race and the dent on the ball surface. (b) Contact between the outer race and the dent on the ball surface.

When the dent of the rolling element is in contact with the inner ring, the contact deformation is defined as:

$$\delta_{DBi} = \begin{cases} r - (\|\chi_j + \rho_{12}\| - R_2), & \text{if } r - \|\chi_j + \rho_{12}\| + R_2 > 0 \\ 0, & \text{else} \end{cases} \quad (29)$$

where ρ_{12} is the vector from the centre of the rolling element to the centre of the radii of the flattened curvature. The projection of the contact force to the radial direction of the rolling element is:

$$F_{DCi} = k_{DCi} \delta_{DBi}^{\frac{3}{2}} \frac{\rho + (x_o - x_i) \cos \theta_j + (y_o - y_i) \sin \theta_j}{\chi_j} \cos(\theta_x - \phi_C), \quad (30)$$

where k_{DCi} is the contact stiffness between the dent and the inner race. The radii of curvature for the rolling element that are taken into account to calculate the contact stiffness are:

$$r_{I1} = \rho_b \quad r_{I2} = \rho_b \quad (31)$$

The contact deformation between the dent and the outer race is given by:

$$\delta_{DBo} = \begin{cases} \|\rho_j + \rho_{12}\| + R_2 - R(\theta), & \text{if } \|\rho_j + \rho_{12}\| + R_2 - R(\theta) > 0 \\ 0, & \text{else} \end{cases} \quad (32)$$

and the contact force in the radial direction of the ball position is given by:

$$F_{DCo} = k_{DCo} \delta_{DBo}^{\frac{3}{2}} \frac{\rho + (x_o - x_i) \cos \theta_j + (y_o - y_i) \sin \theta_j}{\chi_j} \cos(\theta_j - \phi_C) \quad (33)$$

4 Numerical results

In this section the presented model was used to simulate the vibration response of a bearing with different faults during run-up. Whenever the fault is in contact with its mating surface, one of the equations (26)-(33) is used to replace the appropriate equations for the contact force in equations (13)-(16).

The bearing under investigation is **NMB R-1240KK1**, shown in Figure 7(a), whose parameters are given in Table 1. The outer ring is assumed to be closely fitted into another aluminium ring, which represents the housing of the bearing and the under half of the aluminium ring is connected with springs to the fixed pedestal, as shown in Figure 7(b). The aluminium ring is 3mm thick, and is connected with 36 linear springs to the fixed pedestal. The stiffness of the connecting spring is $k_s = 100000$ N/m. In the analysed case a simple support structure was chosen to avoid confusing the bearing vibration with the structural vibration, since the transfer path of the housing could change the vibration signal. The outer ring of the bearing and the aluminium ring is modelled with 72 finite elements. The bearing loads are assumed to be the gravitational load and the unbalanced force. The unbalance of the rotor is $me_u = 2 \times 10^{-5}$ kgm². From the radius of the inner and outer races it is clear that the radial clearance in

Table 1: Geometrical and physical properties used for the rolling-element bearing shown in Figure7(a).

Inner-race radius r	2.754 mm
Outer-race radius R	4.7565 mm
Ball radius ρ_b	1 mm
Inner-race radius curvature r_{II1i}	1.04 mm
Outer-race radius curvature r_{II1o}	1.07 mm
Area of outer race A_{oR}	5.37mm ²
Principal moment of inertia of outer race I_{oR}	0.888 mm ⁴
Radius to the centre of outer race R_C	5.314 mm
Number of balls N_b	7
Ball mass m_b	0.0000329 kg
Mass of inner ring and shaft m_S	0.15 kg
Radial clearance c	5 μ m
Inner contact stiffness k_i	3.828×10^9 N/m
Outer contact stiffness k_o	3.867×10^9 N/m

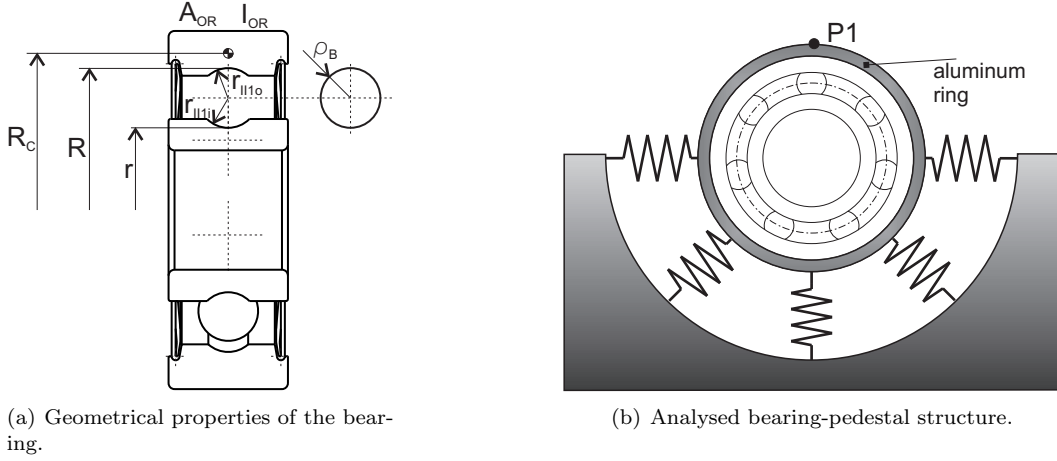


Figure 7: Analysed bearing during run up.

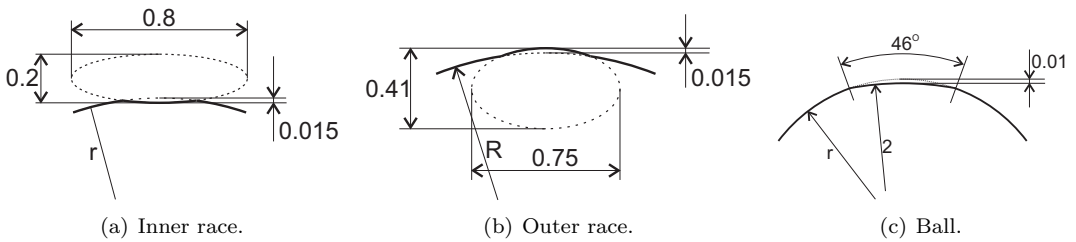


Figure 8: Dent geometry on different bearing components.

the bearing is $c = 5 \mu\text{m}$. The outer ring, the inner ring and the shaft are made from steel. The dynamic response of the bearing will be taken from point **P1**, which is on the top of the aluminium ring, Figure 7(b).

The geometrical properties of the local faults are shown in Figure 8. The faults on the inner race and the ball will rotate and their position will move in and out of the loading zone in the bearing. The fault on the outer race is stationary, and the position of the dent on outer race is very important. Analyses will be made for the dent in the middle of the loading zone, at the bottom of the outer race.

4.1 Initial condition and numerical solution

For the numerical solution the initial conditions and the step size are very important for a successful and economical computational solution. The larger the time step, the faster the computation. On other hand, the time step should be small enough to achieve an adequate accuracy. Due to the very high contact stiffness $k \approx 4 \times 10^9$ N/m, and the very high eigenfrequencies of the outer ring, the first eigenfrequency is at $f_1 \approx 35$ kHz, and the time step in the presented simulation is $\delta t = 1.5 \times 10^{-8}$ s. Since the time step has to be very small so that the explicit Newmark method is stable, the following strategy was used. First, the initial conditions for the following simulation were calculated, where the shaft was held at centre and was released to calculate the equilibrium position of the whole system due to the gravitational load. This calculated equilibrium position will be used in the following simulations to avoid passing the transient vibration due to the release of the shaft from centre, and the shaft can start accelerating immediately.

4.2 Vibration response of the bearing due to local faults during the run-up of the shaft

With the presented model, the vibration response of the roller-element bearing due to a local defect is simulated during the run-up of the shaft. The rotational speed of the shaft ω_S increases linearly with time. The angular acceleration of the shaft is set to $\alpha_S = 20\pi$ rad/s². The vibration signals will be processed in the frequency and time-frequency domains. The basic indicator in the frequency domain is the presence of the characteristic defect frequencies. The characteristic defect frequencies depend on the rotational speed of the shaft and the location of the defect in the bearing. The expressions for the characteristic defect frequencies for the various defect locations are well established [19]. The characteristic defect frequencies for the analysed bearing are listed in Table 2, where f_S is the rotational speed of the shaft, and f_b is the ball's rotational frequency. In the analysed cases the rotational speed of the shaft f_S will be increasing from 0 to 45 Hz.

Table 2: Characteristic defect frequencies for the stationary outer ring.

Outer race defect frequency, f_{oD}	$2.568f_S$
Inner race defect frequency, f_{iD}	$4.432f_S$
Ball defect frequency, $f_{bD} = 2f_b$	$3.488f_S$

In the frequency domain the demodulation or enveloping-based methods offer the greatest reliable diagnostic potential at a constant rotational speed of the shaft. Although the rotational speed of the shaft will change with time, the method will be tested for bearing-fault detection. The general assumption with the enveloping approach is that a measured signal contains low-frequency phenomena that act as the modulator to the high-frequency carrier signal. For the bearing fault, the low-frequency phenomenon is the impact caused by the defect in the bearing; the high frequency is a combination of the natural frequencies of the associated bearing and the surrounding structure of the bearing. The goal of enveloping is to replace the high-frequency oscillation caused by the impact with a single pulse over the entire duration of the impact response. There are several demodulation methods, but the most widely used and well-established of these is the Hilbert transform. Fourier transformation assumes that the signal is periodic, but this is not true due to the changing angular velocity of the shaft, which has the consequence that the occurrence of the impact is never reproduced exactly from one cycle to another. To minimise this effect, only a short period of the damaged bearing signal will be taken for the analysis. The consequence will be that the signal has to be zero padded to increase the frequency domain resolution. However, frequency-based techniques are not suitable for the analysis of non-stationary signals that are generally related to the bearing fault, especially during run-up. Non-stationary signals can be analysed by applying time-frequency domain techniques such as the short-time Fourier transform, the Wavelet transform (WT) and the Hilbert-Huang transform [20, 21]. In fault diagnostics, the WT is the most popular time-frequency domain technique, because it can provide a more flexible, multi-resolution solution than the short-time FT. According to the signal decomposition paradigm, the WT can be classified as the continuous WT (CWT), the discrete WT (DWT) and wavelet packet analysis. For the detection of the present bearing fault the CWT transform will be used. The damaged bearing will produce small amplitudes of vibration in the high frequency band as the response of the bearing and the housing to the impact that is caused by the fault. This high-frequency band has to be known prior to the wavelet analysis. In the analysed case, Figure 7(b), the high-frequency response will be at the eigenfrequency of the bearing/housing-pedestal

system, which is around 8.2 kHz; the eigenfrequency of the shaft is around 11.3 kHz, although this frequency varies due to the changing position of the balls, and the first eigenfrequency of the outer ring with the aluminium ring is around 36 kHz. The existence of vibrations in these frequency bands will be used to identify the bearing faults. The classification of the bearing faults will be made based on the time interval between the repetitive vibrations in the high-frequency band. The time interval between the vibrations in the high-frequency band is determined by the instantaneous rotational frequency of the shaft and the type of bearing fault.

All the envelope analyses will be made for the time signal between 2.3 s and 2.4 s. The angular speed of the shaft during this period of time will linearly change from 21 Hz to 22 Hz. The CWT analysis will be made for the time signal between 2.2 s and 2.5 s, and the rotational speed of the shaft is linearly changing from 20 Hz to 23 Hz. The vibration signal was filtered with a high-pass Butterworth filter, where the cutoff frequency was set to 5 kHz.

4.2.1 Healthy bearing

Bearing components generate vibration signals that are related to the speed of the shaft's rotation, which is changing. Figure 9(a) shows the acceleration response at the point P1. It can be seen that even a perfect bearing will generate vibrations due to the time-varying distribution of the balls relative to the inner and outer races. Figure 9(b) shows the vibration spectrum of the envelope analysis. There are two dominant frequency peaks, one at 21 Hz, which is equal to the frequency of the shaft rotation, and the other at 78 Hz, which is the characteristic defect frequency of the ball.

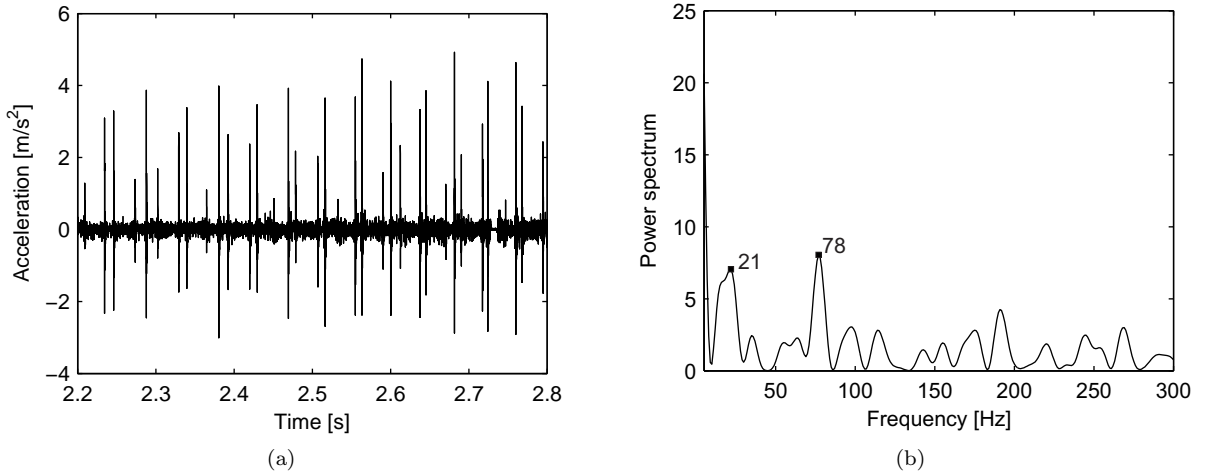


Figure 9: Vibration response of a healthy bearing. (a) Vibration response at point P1. (b) Frequency spectrum of the envelope between 2.3 s and 2.4 s.

The time-frequency plot of the CWT is shown in Figure 10. There are small amplitudes of the vibration in the high-frequency band, most of them around 11 kHz. The time intervals $T_1 \approx 0.0125$ s and $T_2 \approx 0.0099$ s between two consecutive amplitudes indicate the excitation at a high frequency. The time interval T_1 corresponds to the frequency $f_1 = 85.5$ Hz, which is the 4th harmonic of the shaft's instantaneous rotating frequency, which is at $t = 2.24$ s $f_{S1} = 20.3$ Hz. The time interval T_2 corresponds frequency to the $f_2 = 101$ Hz, which would indicate bearing inner-race damage, since the characteristic inner-race defect frequency at an instantaneous shaft speed $f_{Si} = 22.2$ Hz is $f_{iD} = 4.432 \times 22.3 = 98.8$ Hz. Although the bearing is healthy, there is the presence of the characteristic frequency of the inner race fault. This presence is due to the varying position of balls in the bearing and due to the centrifugal loading of the shaft. From the time signal it is clear that the amplitude of the bearing vibration is very small. The conclusion can be made that the bearing has no fault, although in the spectra there are detectable characteristic fault frequencies. If the bearing was faulty, there would also be a second harmonic of the characteristic fault frequency.

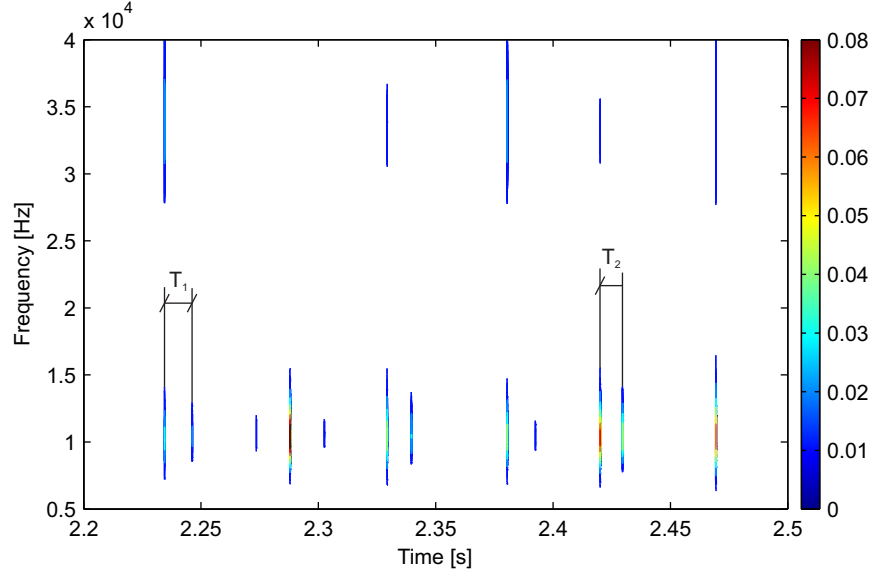


Figure 10: Time-frequency plot of the CWT of the bearing vibration signal in healthy case.

4.2.2 Outer-race fault

Figure 11(a) shows the system response at point $P1$ with one outer-race defect, located in the centre of the loading zone. Every roller will hit the fault while going through the loading zone, which should result in an overwhelmingly dominant frequency at the roller passing frequency. The size and the shape of the defect is shown in Figure 8(a). The vibration at point $P1$ increases dramatically when the ball hits the dent, Figure 11(a), and the peak amplitude is more than two orders higher than in a healthy bearing. In the envelope analysis spectrum, Figure 11(b), there is the presence of the bearing's instantaneous shaft-rotation frequency $f_{Si} = 21$ Hz, and two frequencies that correspond to the characteristic frequency of the outer-race fault $f_{oD} = 2.568 \times 21 = 53.92 \approx 55$ Hz and its second harmonic $2 \times f_{oD} = 107.9 \approx 111$ Hz. The small difference in the frequency is due to the changing shaft-rotation frequency from 21 Hz to 22 Hz in the analysed signal.

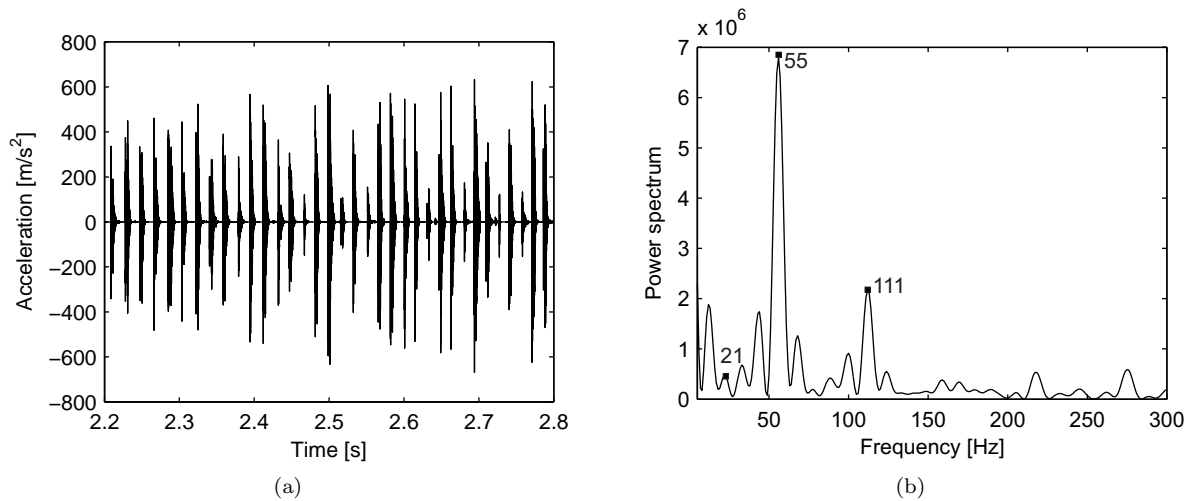


Figure 11: Vibration response of the bearing with the outer-race defect. (a) Vibration response at point $P1$. (b) Frequency spectrum of the envelope between 2.3 s and 2.4 s.

From the time-frequency plot of the CWT, Figure 12, the existence of high-frequency components is detected and their occurrence is repetitive, which indicates the presence of the fault. The high-

frequency response is observed at the first eigenfrequency of the outer race and the eigenfrequency of the outer ring-pedestal system, which is higher in amplitude. The time intervals $T_1 = 0.019$ s and $T_2 = 0.0179$ s correspond to the frequencies $f_1 = 52.6$ Hz and $f_2 = 55.9$ Hz. These two frequencies are correlated with the characteristic frequencies of the outer-race defect, at the shaft's instantaneous rotational frequencies $f_{Si1} = 20.7$ Hz and $f_{Si2} = 21.5$ Hz.

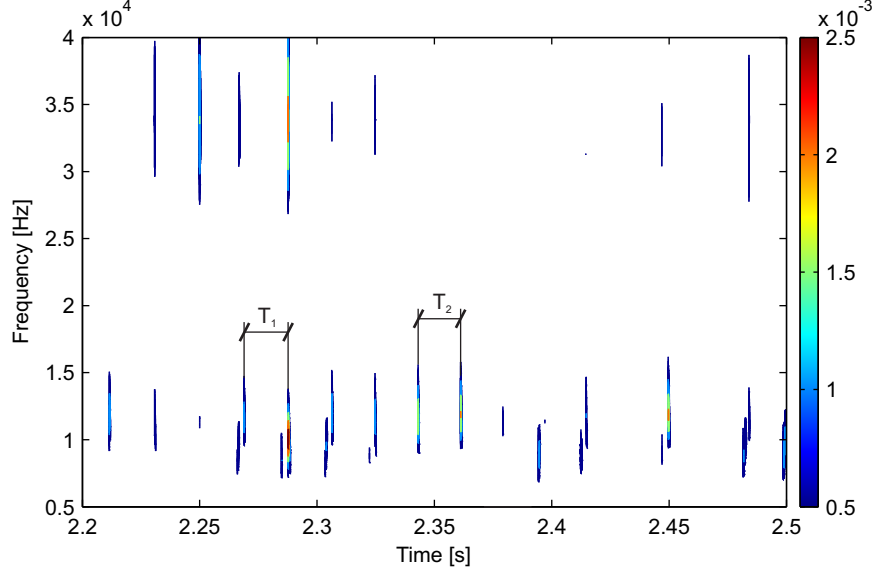


Figure 12: Time-frequency plot of the CWT of the bearing vibration signal with the outer-race fault.

It is clear that each technique can detect the presence of this bearing fault.

4.2.3 Inner-race fault

The defect on the inner race will rotate with the shaft's rotation speed and will go through the loading zone every cycle. The response will be very high when the defect it hits its mating surface in the loading zone. On the other hand, when the defect will be on top the balls it will mostly miss the point defect, and thus shift the dominant faulty frequency to lower bands. For this reason the detection of a fault on the inner race is more challenging than on a fixed race. Figure 13(a) shows the vibration response of the outer ring to the inner-race defect. The size and the shape of the inner-race defect are shown in Figure 8(b).

The envelope spectrum shows a shaft frequency peak at 22 Hz, which is the shaft's rotating frequency. The characteristic frequency of the inner race defect $f_{iD} = 4.432 \times 22 = 97.5$ Hz and its second harmonic $2 \times f_{iD} = 195$ Hz can be clearly identified in the envelope spectrum, Figure 13(b). The small difference in the frequencies is due to the changing speed of the shaft.

From the time-frequency plot of the CWT, Figure 14, the existence of high-frequency components is detected and their occurrence is repetitive, which indicates the presence of the fault. The vibrations of the bearing/pedestal structure appear in the spectrum only when the inner-race fault is in the loading zone. Due to this the interval between two consecutive components of the vibration in the high-frequency band has to be carefully chosen. The time intervals $T_1 = 0.0108$ s and $T_2 = 0.0102$ s correspond to the frequencies $f_1 = 92.6$ Hz and $f_2 = 98.3$ Hz. These two frequencies correlate very well with the characteristic frequencies of the outer-race defect at the instantaneous shaft speeds $f_{Si1} = 20.7$ at $t_1 = 2.27$ s and $f_{Si2} = 22.5$ Hz at $t_2 = 2.45$ s.

It is clear that each technique can detect the presence of this bearing fault, where the time interval in the CWT has to be taken carefully, since only in the loading zone is there the high frequency vibration.

4.2.4 Rolling-element fault

To investigate the vibration response of the bearing to the ball fault, it is assumed that the dent is on the 1st ball. The size and the geometry of the flattened ball are shown in Figure 8(c). The vibration

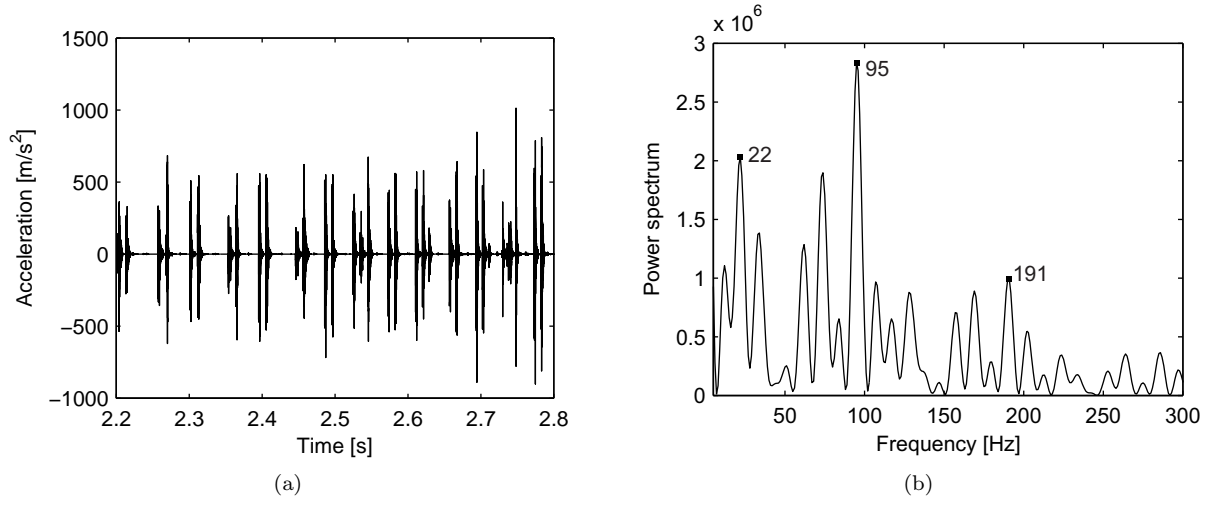


Figure 13: Vibration response of the bearing with the inner-race defect. (a) Vibration response at point P1. (b) Frequency spectrum of the envelope between 2.3 s and 2.4 s.

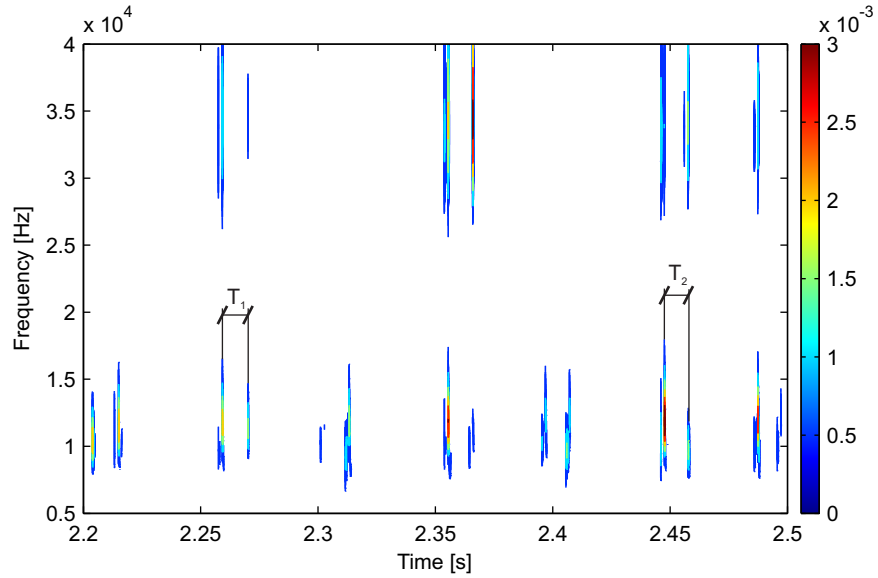


Figure 14: Time-frequency plot of the CWT of the bearing vibration signal with the inner-race fault.

response at point $P1$ is shown in Figure 15(a). The vibration signal is highly modulated, since the high impulsive response is noticed only when the damaged ball is in the loading zone. For this reason the signal taken for the envelope analysis has to be taken carefully. For the spectrum of the envelope analysis the vibration signal is taken from 2.3 s to 2.45 s. With the shorter signal the characteristic defect frequency it hard to identify, but due to a larger change of the shaft's rotation frequency in this time interval, the shaft's rotation frequency is not present in the frequency spectrum of the envelope analysis. From the simulation it is known that the shaft's rotation frequency increases from 21 Hz to 22.5 Hz. However, the characteristic defect frequency of the ball defect $f_{bD} = 3.488 \times 21.5 = 75$ Hz and its second harmonic $2 \times f_{bD} = 150$ Hz can be identified clearly in the envelope-analysis spectrum Figure 15(b).

From the time-frequency plot of the CWT the existence of high-frequency components is detected only when the ball is in the load zone. The time interval between two consecutive amplitudes in the high-frequency band determines the presence of the ball faults. The time intervals $T_1 = 0.0134$ s and $T_2 = 0.0125$ s correspond to the frequencies $f_1 = 74.6$ Hz and $f_2 = 80$ Hz, which are characteristic frequencies of the ball defect at the shaft's instantaneous rotational frequencies $f_{S1} = 21$ Hz at $t_1 = 2.3$

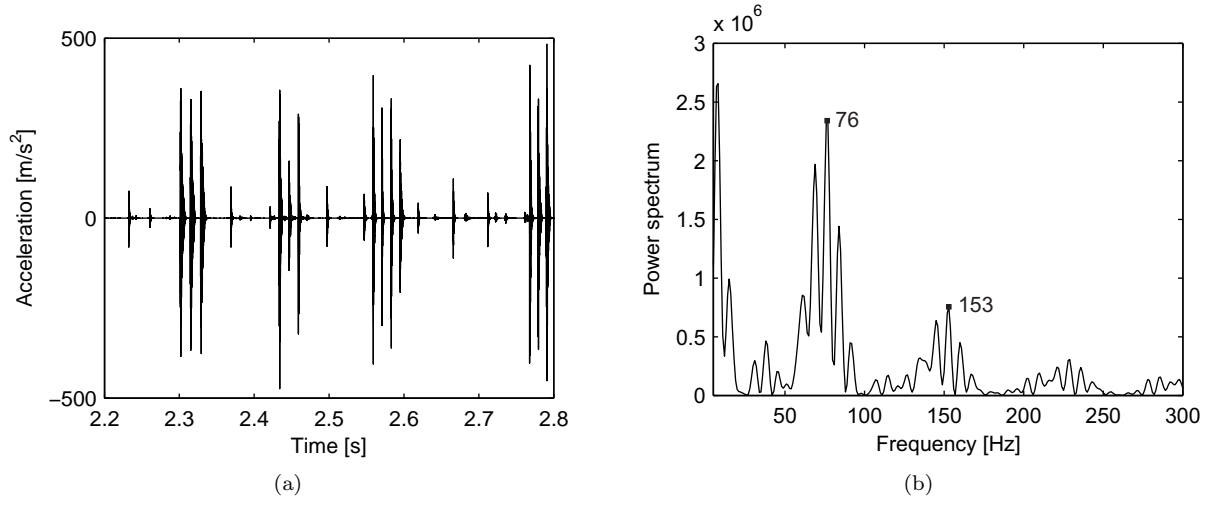


Figure 15: Vibration response of the bearing with the ball defect. (a) Vibration response at point P1. (b) Frequency spectrum of the envelope between 2.25 s and 2.25 s.

s and $f_{Si2} = 22.5$ Hz at $t_2 = 2.45$ s.

It is clear that each technique can detect the presence of a ball fault. However, in the envelope analysis, taking the wrong time interval of the analysed signal can lead to a frequency shift and the ball fault cannot be identified. It is clear that the CWT is better in this case, since the analysed time interval can be taken to be arbitrary.

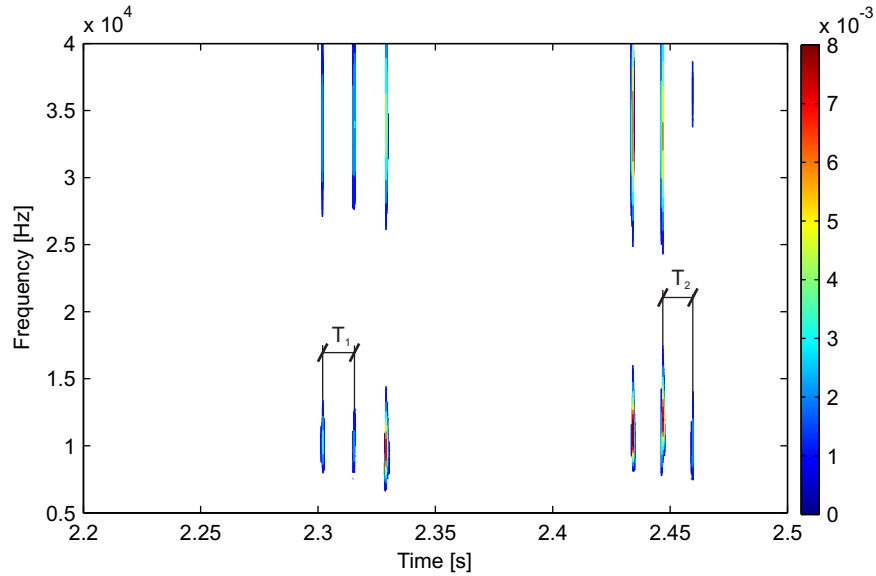


Figure 16: Time-frequency plot of the CWT of the bearing vibration signal with the ball fault.

5 Conclusion

A comprehensive model of a ball bearing is developed to obtain the vibration response due to localised defects. For the purpose of simplification, the inner ring of the bearing has only 2 DOF and the centrifugal load effects are included. The proposed model includes several new considerations. The outer ring is deformable and is modelled with finite elements, and can be coupled with an arbitrary housing structure if it is discretized with finite elements. The contact force between the outer race and the ball is moving

within the finite element continuously, and due to this the finite element can be larger and the final model is computationally less demanding. The contact properties are described with detailed geometrical properties and small changes in the contact stiffness are taken into account.

The developed bearing model is used to simulate the vibration response of the bearing/pedestal system due to different local faults, while the shaft's rotational frequency is increasing. Although the rotational frequency is non-stationary, the envelope analysis method could identify all the local bearing defects. The time interval for the envelope analysis has to be taken carefully, since the defect on the bearing element has to be in the loading zone in that time interval, but the time interval has to be short enough so that there is only a small change in the shaft's rotating frequency. The signal used for the envelope analysis has to be zero padded to have a sufficient frequency resolution, where we have to be aware of the limitations and consequences of zero padding. On other hand, the CWT gives the same results, where the analysed time interval can be taken as arbitrary to identify the bearing faults.

References

- [1] P.D. McFadden and J.D. Smith. Model for the vibration produced by a single point defect in a rolling element bearing. *Journal of Sound and Vibration*, 96:69–82, 1984.
- [2] P.D. McFadden and J.D. Smith. The vibration produced by multiple point defect in a rolling element bearing. *Journal of Sound and Vibration*, 98:263–273, 1985.
- [3] N. Tandon and A. Choudhury. An analytical model for the prediction of the vibrations response of rolling element bearings due to a localized defect. *Journal of Sound and Vibration*, 205:275–292, 1997.
- [4] A. Choudhury and N. Tandon. Vibration response of rolling element bearings in a rotor system to a local defects under radial load. *Journal of Tribology*, 128:251–261, 2006.
- [5] C.S. Sunnersjo. Varying compliance vibrations of rolling element bearings. *Journal of Sound and Vibration*, 3:363–373, 1978.
- [6] A. Rafsanjani, S. Abbasion, A. Farshidianfar, and H. Moeenfar. Nonlinear dynamic modeling of surface defects in rolling element bearing systems. *Journal of Sound and Vibration*, 319:1150–1174, 2009.
- [7] A. Liew, N.Feng, and E.J. Hahn. Transient rotor dynamic modelling of rolling element bearing systems. *ASME Journal of Engineering for Gas Turbines and Power*, 124:984–991, 2002.
- [8] N. S. Feng, E. J. Hahn, and R. B. Randall. Using transient analysis software to simulate vibrations signals due to rolling element bearing defects. *Proceedings of the 3rd Australian Congress on Applied MEchanics*, pages 689–694, 2002.
- [9] H. Arslan and N. Akturk. An investigation of rolling element vibrations caused by local defects. *Journal of Tribology*, 130, 2008.
- [10] J. Sopianen and A. Mikola. Dynamic model of a deep-groove ball bearing including localized and distributed defects—part 1: theory. *Proceedings of the Institution of Mechanical Engineers K—Journal of Multi-body Dynamics*, 217:201–211, 2003.
- [11] J. Sopianen and A. Mikola. Dynamic model of a deep-groove ball bearing including localized and distributed defects—part 2: implementation and results. *Proceedings of the Institution of Mechanical Engineers K—Journal Multi-body Dynamics*, 217:213–223, 2003.
- [12] Z. Kiral and H. Karagulle. Simulation and analysis of vibration signals generated by rolling element bearing with defects. *Tribology International*, 36:667–678, 2003.
- [13] S.P. Harsha. The effect of ball size variation on nonlinear vibrations associated with ball bearings. *Proceedings of the Institution of Mechanical Engineers, Part K: Journal of Multi-body Dynamics*, 218:191–210, 2004.

- [14] S.P. Harsha. Nonlinear dynamic analysis of rolling element bearings due to cage run-out and number of balls. *Journal of Sound and Vibration*, 289:360–381, 2006.
- [15] M. Cao and J. Xiao. A comprehensive dynamic model of double-row spherical roller bearing-model development and case studies on surface defects, preloads, and radial clearance. *Mechanical Systems and Signal Processing*, 22:467–489, 2008.
- [16] P. Raveendranathh, G. Singh, and B. Pradhan. A two-noded locking-free shear flexible curved beam element. *Int. J. for Numerical Methods in Engineering*, 44:265–280, 1999.
- [17] S.P. Harsha. Nonlinear dynamic analysis of an unbalanced rotor supported by roller bearing. *Chaos, Solitons and Fractals*, 26:47–66, 2005.
- [18] T. A. Harris. *Rolling bearing analysis*. John Wiley and Sons, 2001.
- [19] N. Tandon and A. Choudhury. A review of vibration and acoustic measurement methods for the detection of defects in rolling element bearings. *Tribology International*, 32:469–480, 1999.
- [20] R.X. Gao and R. Yan. Non-stationary signal processing for bearing health monitoring. *International Journal of Manufacturing Research*, 1:18–40, 2006.
- [21] T. Kijewski-Correa and A. Kareem. Efficacy of Hilbert and wavelet transforms for time-frequency analysis. *Journal of Engineering Mechanics*, pages 1037–1049, 2006.